

Potential model calculations of parity violation in proton-proton scattering

D. E. Driscoll and G. A. Miller

Institute for Nuclear Theory, Department of Physics, University of Washington, Seattle, Washington 98195

(Received 24 June 1988)

The proton-proton parity-violating analyzing power is calculated at laboratory energies up to 1000 MeV using a parity-violating weak meson-exchange potential with form factors and coupling constants consistent with the nonrelativistic Bonn potential. A real distorted-wave Born-approximation formulation of the weak scattering amplitude is introduced using real standing waves with distortions by Coulomb and strong interactions. This formulation includes a new and simplified expression for the S matrix in terms of strong and real weak amplitudes. The form-factor contributions to the weak potential significantly reduce the overall magnitude of the analyzing power, but do not qualitatively affect the relative energy or angular dependence. Results using, alternatively, Paris, Reid soft-core, Hamada-Johnston, and pure Coulomb distorted waves with the same weak potential are compared. The angular and total analyzing powers are calculated with long-range Coulomb contributions for scattering and transmission experiments. The long-range Coulomb effects can be removed, leading to a reduced analyzing power \hat{A} that depends only on short-range forces.

I. INTRODUCTION

Parity-violation nucleon-nucleon scattering and transmission experiments are providing increasingly sensitive tests of the parity-violating hadronic interactions.¹⁻⁷ As the set of measurements is expanding and improving, a corresponding increase of attention to the details of the theoretical calculations is required. In 1973, Brown, Henley, and Krejs⁸ calculated the analyzing power using nonrelativistic strong and parity-violating potentials. Oka⁹ performed a relativistic calculation, but neglected the strong distortion of the nucleon-nucleon wave functions. In 1979, Desplanques, Donoghue, and Holstein¹⁰ estimated, using the Weinberg-Salam model and quark bag wave functions, the parity-violating meson coupling constants. Adelberger and Haxton have published a review of the subject of parity violation in nucleon-nucleon interactions.¹¹ Since Brown, Henley, and Krejs published their results, improved potential models, particularly the Bonn meson-field-theoretic potential, have been developed, and the data base of conventional hadronic scattering measurements, which determines the strong on-shell t -matrix elements, has improved.

We present new theoretical results for the proton-proton analyzing power which sharpen and update the calculations of Brown, Henley, and Krejs. Our principal result is a new distorted-wave treatment [Eq. (2.4)] which allows the on-shell strong interaction effects (including inelasticities) to be treated in a model-independent manner. The only quantity that depends on the off-shell strong interaction is the weak r matrix, \hat{r}_W , in Eq. (A7), which (neglecting inelasticities) is real. The number of parameters depending on the off-shell strong interactions is thereby minimized. In addition, Eq. (2.4) is simple in form and independent of the S -matrix parametrization. We use this formulation to include recent nucleon-

nucleon strong potentials (and phase shifts), and the influence of modern strong vertex functions on parity-violating (PV) potentials. Furthermore, a careful treatment of Coulomb effects is motivated and presented.

Here is an outline of the remainder of the paper. In Sec. II, we define the compact t - and r -matrix formalism, and formulate an alternative to Watson's theorem¹²⁻¹⁴ using the weak reaction matrix. In Sec. III, we study the Coulomb contributions to the analyzing power observables for scattering and transmission experiments. The derivation of a nonrelativistic potential from meson field theory, using Desplanques, Donoghue, and Holstein parity-violating constants, and with coupling constants and form factors consistent with the Bonn potential, is described in Sec. IV. Section V contains results of nonrelativistic distorted-wave Born approximation (DWBA) calculations using the Bonn and alternative strong potentials, as well as results to exemplify and conclude the work of Secs. III and IV. Section VI is a summary. The Appendix explicitly describes the DWBA integrations.

II. FORMALISM

Define the nucleon-nucleon scattering operator T as

$$T(E) = V + V \left[\frac{1}{E^+ - H_0} \right] T(E),$$

where V is the potential. The reaction matrix¹⁵ $R(E)$ is

$$R(E) = V + VP \frac{1}{E - H_0} R(E),$$

with T and R related by

$$T(E) = R(E) + R(E)(-i\pi)\delta(E - H_0)T(E). \quad (2.1a)$$

Our goal in this section is to derive a DWBA treatment which employs R . To this end we employ a compact no-

tation. The on-shell matrix elements $t_{l's';ls}^j$ and $r_{l's';ls}^j$ (in which l , s , and j are the usual angular momentum quantum numbers) are represented simply as t and r . Then we can write Eq. (2.1a) on shell in the more compact form

$$t = r + irt. \quad (2.1b)$$

For simplicity, we imply conventional matrix algebra in the $(ls)j$ space whenever matrix indices are suppressed. The matrix t can be determined from r , or r from t , by solving Eq. (2.1b). The s matrix is given by

$$s = 1 + 2it. \quad (2.2)$$

Time-reversal invariance implies that t , r , and s are symmetric. (The spin and angular momentum phase conventions must be chosen appropriately.) Below the inelastic threshold, s is unitary and r is real symmetric. For example, in an uncoupled channel l , $s = \exp(2i\delta_l)$, $t = \exp(i\delta_l)\sin\delta_l$, and $r = \tan\delta_l$.

For proton-proton scattering, we define Coulomb-reduced quantities \hat{s} , \hat{t} , and \hat{r} related to s , t , and r by

$$s = e^{i\sigma}\hat{s}e^{i\sigma}, \quad (2.3a)$$

$$t = \sin\sigma e^{i\sigma} + e^{i\sigma}\hat{t}e^{i\sigma}, \quad (2.3b)$$

$$r = (\sin\sigma + \cos\sigma\hat{r})(\cos\sigma - \sin\sigma\hat{r})^{-1}. \quad (2.3c)$$

Here, σ denotes the diagonal matrix of Coulomb phase shifts. We define

$$\sigma_{l's';ls}^j = \delta_{l'l}\delta_{s's}\sigma_l, \quad \sigma_l = \arg\Gamma(l+1+\eta),$$

and $\eta = \alpha c/v_L$, with α the fine-structure constant, c the speed of light, and v_L the laboratory velocity calculated relativistically from the laboratory beam energy. The matrices \hat{s} , \hat{t} , and \hat{r} satisfy relationships analogous to Eqs. (2.1) and (2.2):

$$\hat{t} = \hat{r} + i\hat{r}\hat{t}, \quad (2.1')$$

$$\hat{s} = 1 + 2i\hat{t}. \quad (2.2')$$

\hat{s} , \hat{t} , and \hat{r} represent the deviation from pure Coulombic scattering, and converge rapidly with increasing partial waves. For $j \gg kd$, with k the relative wave number and d the range of nuclear interactions, $\hat{s}_{l's';ls}^j \rightarrow \delta_{l'l}\delta_{s's}$, $\hat{t}_{l's';ls}^j \rightarrow 0$, and $\hat{r}_{l's';ls}^j \rightarrow 0$.

Any amplitude can be separated explicitly into parity-conserving and parity-violating terms. For simplicity, we indicate these terms with subscripts S and W . For example, $\hat{t} = \hat{t}_S + \hat{t}_W$ and $\hat{r} = \hat{r}_S + \hat{r}_W$. The parity-violating observables are derived from \hat{t}_S and \hat{t}_W . The matrix \hat{t}_S , the strong scattering amplitude, is relatively well determined by conventional scattering data, and does not contain information on parity violation. The degrees of freedom in \hat{t}_W depending on parity-violating interactions can be reduced to a simpler form, \hat{r}_W , which, below inelastic threshold, is real. From Eq. (2.1'), one obtains, to first order in \hat{r}_W ,

$$\hat{t}_W = (1 + i\hat{t}_S)\hat{r}_W(1 + i\hat{t}_S). \quad (2.4)$$

With no Coulomb force, $r_W = \hat{r}_W$, and the elements of r_W are the partial-wave components of plane-wave matrix

elements of

$$R_W = \left[1 + R_S P \frac{1}{E - H_0} \right] V_W \left[1 + P \frac{1}{E - H_0} R_S \right].$$

The plane-wave matrix elements are real distorted standing-wave matrix elements of V_W . With the Coulomb force, \hat{r}_W is, as given in the Appendix, Eq. (A7), a matrix element of V_W with wave functions distorted by both Coulomb and strong forces. Equation (A7) is consistent with \hat{r}_W defined above, provided the wave functions have the real Coulomb standing-wave boundary conditions specified in Eq. (A5b). Notice \hat{r}_W changes parity, so $l' = l \pm 1$. \hat{r}_W contains, for identical nucleons, just one independent real element for $j=0$, and two real elements for each higher even j .

In principle, \hat{t}_W can be calculated directly from the DWBA integral Eq. (A8), using model-derived incoming and outgoing distorted waves $u^{(-)}$ and $u^{(+)}$, rather than from Eqs. (2.4) and (A7). However, because model-derived values can disagree with empirical values for \hat{t}_S , the two methods will generally disagree. The method using \hat{r}_W with empirical values for \hat{t}_S [Eqs. (2.4) and (A7)] is preferred. Below inelastic threshold, \hat{r}_W is real, and so contains fewer model-dependent parameters than \hat{t}_W . The additional degrees of freedom in \hat{t}_W are determined by the on-shell strong interaction quantities \hat{t}_S .

As a consequence, for example, consider the zero crossing energy of the analyzing power. The helicity-dependent cross section depends only on $\text{Im}\hat{t}_W$. The zero crossing energy of the 1S_0 - 3P_0 contribution to the cross section then only depends on the factors $(1 + i\hat{t}_S)$, since \hat{r}_W is real, and so is most accurately determined from empirical values for \hat{t}_S . Second, above threshold, inelastic contributions to \hat{t}_W in the strong factors $1 + i\hat{t}_S$ can be included by using empirical inelastic parameters in \hat{t}_S .

The factorization of \hat{t}_W in Eq. (2.4) is different from the factorization for \hat{t}_W (or $\hat{s}_W = 2i\hat{t}_W$) derived by Watson.¹²⁻¹⁴ In the absence of strong-channel couplings, the strong factors $(1 + i\hat{t}_S)$ in Eq. (2.4) equal $\cos\delta e^{i\delta}$, with δ a phase shift. The strong factors in Watson's parametrization are, instead, $e^{i\delta}$, which can lead to a different result when empirical and model-derived phases disagree. Henley¹² recently generalized Watson's theorem for coupled channels with inelastic contributions. Henley's parametrization also differs from Eq. (2.4). The advantage of Eq. (2.4), besides its simplicity, is its freedom from arbitrary choices for the parametrization of \hat{t}_W . The factorization of \hat{t}_W in Eq. (2.4) is determined naturally by the relationship, Eq. (2.1'), of \hat{t} to \hat{r} , or, as shown in the Appendix, by the outgoing and standing-wave boundary conditions of Eqs. (A5). Below threshold, \hat{t}_W , given by Eq. (2.4), automatically satisfies the unitary condition for first-order weak corrections to the S matrix, because \hat{r}_W is real.

III. COULOMB CONTRIBUTIONS TO THE ANALYZING POWER

In proton-proton scattering, the parity-violating observables O_{PV} depend on the interference between

parity-conserving f and parity-violating f_{PV} amplitudes: $\mathcal{O}_{\text{PV}} \propto \text{Re} f f_{\text{PV}}^*$. Measurements are often made at forward angles where the Coulomb contribution to f diverges. Therefore, it is necessary to treat Coulomb effects in \mathcal{O}_{PV} carefully. To our knowledge, no such treatment exists for both angular distribution (scattering) and transmission experiments. Therefore, Coulomb effects are examined here.

We consider scattering and transmission parity-violating experiments. In practice, both types of experiment use a polarized proton beam on an unpolarized target and alternate the beam polarization to determine the helicity dependence of a cross section. When both parti-

cles in the reaction are charged, we must, in general, take account of the long-range Coulomb force.

In parity-violating scattering experiments, the detector, assumed cylindrically symmetric, subtends a range of nonforward scattering angles, say from θ_1 to θ_2 . Due to the large scattered currents in these experiments, particles cannot be individually counted and analyzed. Instead, the detector measures the collective current of all particles scattered into the detector. When inelastically scattered particles are negligible, the experiment measures a cross section related to the elastic scattering amplitude $M = M_C + M_N$, where

$$M_{N_s m'_s; s m_s}(\Omega) = \frac{1}{k} \sum_{j'l'} Y_{l'm_s - m'_s}(\Omega) \sqrt{4\pi(2l+1)} C_{l's'j}^{m_s - m'_s m'_s m_s} C_{lsj}^{0m_s m_s} [1 + (-1)^{l+s}] e^{i\sigma_l} \hat{t}_{l's'; ls} e^{i\sigma_l}. \quad (3.1a)$$

M_C is the symmetrized pure Coulomb scattering amplitude,

$$M_{C_s m'_s; s m_s}(\Omega) = \frac{1}{k} \delta_{s's} \delta_{m'_s m_s} \sum_{l=0}^{\infty} P_l(\cos\theta) (2l+1) [1 + (-1)^{l+s}] \sin\sigma_l e^{i\sigma_l}, \quad (3.1b)$$

$C_{lsj}^{m_l m_s m_j}$ are the Clebsh-Gordan coefficients, and $Y_{lm_l}(\theta, \phi) = Y_{lm_l}(\Omega)$ are the spherical harmonics.¹⁶ The differential cross sections $\sigma_+(\theta)$ and $\sigma_-(\theta)$ for positive and negative beam polarization states are simple linear combinations of the spin cross sections,

$$\sigma_{s' m'_s; s m_s}(\Omega) = |M_{s' m'_s; s m_s}(\theta, \phi)|^2. \quad (3.2)$$

For spin states quantized along the beam direction, the cross sections are independent of ϕ .

The angular analyzing power is defined as the ratio

$$A(\theta) = \frac{\sigma_+(\theta) - \sigma_-(\theta)}{\sigma_+(\theta) + \sigma_-(\theta)}. \quad (3.3)$$

The scattering experiment then measures a weighted average of $A(\theta)$,

$$A|_{\theta_1}^{\theta_2} = \frac{\int_{\theta_1}^{\theta_2} d\Omega \sigma(\theta) A(\theta)}{\int_{\theta_1}^{\theta_2} d\Omega \sigma(\theta)}, \quad (3.4)$$

with $\sigma(\theta) = [\sigma_+(\theta) + \sigma_-(\theta)]/2$. Coulomb effects appear explicitly through M_C , explicitly through the Coulomb phases multiplying \hat{t} in Eq. (3.1), and implicitly through \hat{t} itself. The reduced scattering matrix \hat{t} is influenced by the Coulomb field only inside the range of the hadronic interaction.

Transmission experiments, contrary to scattering experiments, measure the transmission of a polarized beam in the target. A cross section is inferred from the transmission measurement. Beam particles absorbed or scattered by angles greater than some critical angle θ_d are removed from the beam; these events reduce the observed transmission and add to the inferred cross section. Beam particles scattered to angles less than θ_d are not distinguished from the beam and do not contribute to the cross section. Particles emitted by inelastic processes in

directions less than θ_d , which we neglect, would reduce the inferred cross section.

For the following, let us "switch off" the Coulomb force, or suppose that one particle in the reaction is neutral. Let σ_+ and σ_- be the total cross sections for positive and negative beam polarization states. Parity-violating experiments actually measure $\sigma_+|_{>\theta_d}$ and $\sigma_-|_{>\theta_d}$, the total cross sections excluding processes with scattering angles less than θ_d . When the small-angle contributions are small, $\sigma_+|_{>\theta_d} \approx \sigma_+$ and $\sigma_-|_{>\theta_d} \approx \sigma_-$. Then, by alternating the beam polarization, the experiment determines

$$A = \frac{\sigma_+ - \sigma_-}{\sigma_+ + \sigma_-}. \quad (3.5)$$

The cross sections σ_+ and σ_- are simple linear combinations of the forward-angle scattering amplitudes $M_{s' m'_s; s m_s}(0)$. In particular,

$$\sigma_+ - \sigma_- = \frac{2\pi}{k} \text{Im}[M_{00;10}(0) + M_{10;00}(0)], \quad (3.6)$$

$$\sigma_+ + \sigma_- = \frac{2\pi}{k} \text{Im}[2M_{11;11}(0) + M_{10;10}(0) + M_{00;00}(0)].$$

When both beam and target particles are charged, the small-angle scattering contributions are large, $\sigma_+|_{>\theta_d}$ and $\sigma_-|_{>\theta_d}$ diverge as $\theta_d \rightarrow 0$, and the forward scattering amplitude is undefined. Holdeman and Thaler¹⁷ have developed an alternative form of Eq. (3.6) for experiments with charged interacting particles. For small θ_d , $\sigma_+|_{>\theta_d}$ and $\sigma_-|_{>\theta_d}$ are again determined by the forward nuclear scattering amplitude, but by Eqs. (3.9) and (3.12) which follow.

For simplicity, let us now neglect spin. Before calculating the cross sections $\sigma|_{>\theta_d}$ that depend on θ_d , consid-

er the definition of Holdeman and Thaler of the total nuclear cross section σ_N . Their cross section is, in some sense, the true cross section measured relative to the pure Coulomb cross section. The nuclear cross section σ_N , however, is not the Coulomb-reduced cross section $\hat{\sigma}$ which we define later. In the literature, $\hat{\sigma}$ is often called the "nuclear cross section," confusing it with σ_N .

Of course, σ_N is not simply $\sigma - \sigma_C$. For an idealized infinite-range Coulomb force, σ and σ_C are undefined. In any physical circumstance, however, the Coulomb field is shielded, and the cross sections are large, not infinite. Let σ^R be the full cross section, and σ_C^R the pure Coulombic cross section for a Coulomb field shielded at radius R . We require that σ_N be insensitive to R . As shown by Holdeman and Thaler, however, σ^R contains nuclear-shielding interference contributions $\sigma^{\ln kR}$ that vary as the logarithm of R . The logarithmic term is undetected by instruments with angular resolution $\Delta\theta \gg (kR)^{-1}$; having no practical significance, we remove $\sigma^{\ln kR}$ with σ_C^R from the observed cross section:

$$\sigma_N \equiv \lim_{R \rightarrow \infty} (\sigma^R - \sigma_C^R - \sigma^{\ln kR}). \quad (3.7)$$

Then, by separate applications of the optical theorem to σ^R and σ_C^R ,

$$\sigma_N = \frac{4\pi}{k} \text{Im} M_N(0). \quad (3.8)$$

Transmission experiments do not directly measure σ_N , but measure

$$\sigma|_{>\theta_d} = \sigma_N|_{>\theta_d} + \sigma_C|_{>\theta_d}, \quad (3.9)$$

where

$$\sigma_N|_{>\theta_d} = \sigma_{\text{inel}} + \int_{\theta_d}^{\pi/2} d\Omega |M_N|^2 + 2 \text{Re} \int_{\theta_d}^{\pi/2} d\Omega M_C^* M_N, \quad (3.10)$$

and where σ_{inel} is the total inelastic cross section. Generally, σ_{inel} is unknown, and we need Eq. (3.8) to determine $\sigma_N|_{>\theta_d}$ or $\sigma|_{>\theta_d}$; that is,

$$\sigma_N|_{>\theta_d} = \sigma_N - \int_0^{\theta_d} d\Omega |M_N|^2 - 2 \text{Re} \int_0^{\theta_d} d\Omega M_C^* M_N. \quad (3.11)$$

Note, however, the point Coulomb function M_C oscillates indefinitely at small angles θ . Interpreted literally, the last integral in Eq. (3.11) is undefined at its lower limit. However, by implicitly taking the limit $R \rightarrow \infty$ after inserting shielded amplitudes and performing all other operations, Eq. (3.11) is correct. This procedure is performed in practice by integrating term by term in the partial-wave sum of M_C .

Suppose θ_d is sufficiently small that $M_N(\theta) \approx M_N(0)$ for $\theta < \theta_d$, and that the small-angle integral of $|M_N|^2$ is negligible; then, by Eq. (3.7), (3.10), (3.11), and the shielding-limit procedure, we deduce

$$\sigma_N|_{>\theta_d} = \frac{4\pi}{k} \text{Im} [e^{2i[\eta \ln \sin(\theta_d/2) - \sigma_0]} M_N(0)]. \quad (3.12)$$

Results given by Eqs. (3.8) and (3.12) differ by a phase depending on η and θ_d . At arbitrarily small angles θ_d , $\sigma_N|_{>\theta_d}$ oscillates indefinitely. For sufficiently large η , nevertheless, σ_N can be extrapolated from transmission measurements, that is, from $\sigma|_{>\theta_d}$.¹⁸ Goldhaber¹⁹ has used Eq. (3.12) to estimate Coulomb effects in parity-violating transmission experiments.

Now consider, as an alternative to σ_N , the reduced cross section $\hat{\sigma}$ defined by

$$\hat{\sigma} = \sigma_{\text{inel}} + \int_0^{\pi/2} d\Omega |\hat{M}|^2, \quad (3.13)$$

where (with spin),

$$\begin{aligned} \hat{M}_{s'm_s'; sm_s}(\Omega) &= \frac{1}{k} \sum_{j'l'} Y_{l'm_s - m_s'}(\Omega) \sqrt{4\pi(2l+1)} \\ &\times C_{l's'j}^{m_s - m_s' m_s'} C_{lsj}^{0m_s m_s} \\ &\times [1 + (-1)^{l+s}] \hat{t}_{l's'; ls}. \end{aligned} \quad (3.14)$$

Then (again neglecting spin),

$$\hat{\sigma} = \frac{4\pi}{k} \text{Im} \hat{M}(0). \quad (3.15)$$

Notice $\hat{\sigma}$ bears the same formal relationship to \hat{M} and \hat{t} in Eqs. (3.14) and (3.15) as σ bears to M and t in Eq. (3.6), with the Coulomb force absent. While σ_N , being the difference of two cross sections, can be negative, each partial-wave contribution to $\hat{\sigma}$ is non-negative, and so $\hat{\sigma}$ is non-negative. Also notice that

$$\sigma_N = \hat{\sigma} + 2 \text{Re} \int_0^{\pi/2} d\Omega M_C^* M_N. \quad (3.16)$$

The Coulomb-nuclear interference term is a manifestation of long-range Coulomb scattering. On the other hand, \hat{t} and $\hat{\sigma}$ are sensitive to the Coulomb field only inside the range of nuclear interactions. While σ_N and $\sigma_N|_{>\theta_d}$ properly represent experimental or long-range observations, the reduced cross section $\hat{\sigma}$ is sensitive only to the short-range properties of particles. That is, $\hat{\sigma}$ is the intrinsic measure of the cross section. For the intrinsic measure of parity violation in scattering reactions, we define the reduced parity-violating analyzing power,

$$\hat{A} = \frac{\hat{\sigma}_+ - \hat{\sigma}_-}{\hat{\sigma}_+ + \hat{\sigma}_-}. \quad (3.17)$$

IV. NONRELATIVISTIC STRONG AND WEAK POTENTIAL MODELS

To obtain the elements of the parity-violating reaction matrix \hat{r}_W , we calculate, as described in the Appendix, the real DWBA matrix elements using nonrelativistic strong and weak potentials V_S and V_W . An objective of our work is to calculate the parity-violating analyzing power using potentials V_S and V_W that are mutually and consistently derived from meson field theory. To that end, we adopt the coordinate-representation Bonn potential²⁰ for V_S , and a parity-violating rho- and omega-

exchange potential with Bonn coupling constants and form factors for V_W .

The Bonn potential is the simplified one-boson-exchange coordinate-space version of the full momentum-space Bonn potential. Bonn incorporates six mesons, including a fictitious sigma meson to simulate two-pion and pi-rho exchanges. Monopole form factors, with one cutoff parameter per meson type, regularize the potential and represent, crudely, the short-range interactions.

Each meson-exchange graph has two meson-nucleon vertices. In graphs contributing to V_W , one vertex is weak (parity violating), and one is strong (parity conserving). In graphs contributing to V_S , both vertices are strong. For each meson type, we apply the same Bonn form factor (for lack of better knowledge) to both strong and weak vertices. Then, for each graph i contributing a term V_i to V_S or V_W , the form factors modify V_i by the

$$V_{W\pi}^{\text{pt}}[m_\pi; r] = 0,$$

$$V_{W\rho}^{\text{pt}}[m_\rho; r] = -g_\rho h_\rho^{pp} \left[(1 + \mu_V) i(\sigma_1 \times \sigma_2) \cdot \left[\frac{-i\nabla}{m_N}, \frac{e^{-m_\rho r}}{4\pi r} \right] + (\sigma_1 - \sigma_2) \cdot \left\{ \frac{-i\nabla}{m_N}, \frac{e^{-m_\rho r}}{4\pi r} \right\} \right],$$

$$V_{W\omega}^{\text{pt}}[m_\omega; r] = -g_\omega h_\omega^{pp} \left[(1 + \mu_S) i(\sigma_1 \times \sigma_2) \cdot \left[\frac{-i\nabla}{m_N}, \frac{e^{-m_\omega r}}{4\pi r} \right] + (\sigma_1 - \sigma_2) \cdot \left\{ \frac{-i\nabla}{m_N}, \frac{e^{-m_\omega r}}{4\pi r} \right\} \right].$$

Here, $\mathbf{r} = \mathbf{r}_1 - \mathbf{r}_2$, $\mathbf{p} = -i\nabla = (\mathbf{p}_1 - \mathbf{p}_2)/2$, and h_ρ^{pp} and h_ω^{pp} are the linear combinations of DDH parameters determined by evaluating isospin operators in the proton-proton system:

$$h_\rho^{pp} = h_{\rho_0} + h_{\rho_1} + \frac{1}{\sqrt{6}} h_{\rho_2},$$

$$h_\omega^{pp} = h_{\omega_0} + h_{\omega_1}. \quad (4.3)$$

The DDH "best" values are $h_\rho^{pp} = -15.47 \times 10^{-7}$ and $h_\omega^{pp} = -3.04 \times 10^{-7}$ and are uncertain by roughly $\pm 200\%$. The pion contribution vanishes due to charge-parity (CP) invariance. Notice that the rho and omega Yukawas are essentially equal, since m_ρ and m_ω are very nearly equal. The rho and omega potentials are then linearly independent only because the anomalous moments, and to a small extent the cutoff parameters, are not equal. For consistency with the Bonn model, we apply the Bonn regularization [Eq. (4.1)] to V_W , and use Bonn masses, coupling constants, and cutoff parameter values in Eqs. (4.1) and (4.2). h_ρ^{pp} and h_ω^{pp} are then the only independent parameters.

V. NUMERICAL RESULTS

Results of the nonrelativistic one-boson-exchange calculations of the analyzing power are presented in Figs. 1–12. All the results use the parity-violating potential defined in Sec. IV with DDH "best values" for the parity-violating parameters h_ρ^{pp} and h_ω^{pp} .

Our nominal results for the reduced total analyzing

same prescription,²⁰

$$V_i(r) = V_i^{\text{pt}}[m_i; r] - \frac{(\Lambda_i + \epsilon)^2 - m_i^2}{4\Lambda_i\epsilon} V_i^{\text{pt}}[\Lambda_i - \epsilon; r] + \frac{(\Lambda_i - \epsilon)^2 - m_i^2}{4\Lambda_i\epsilon} V_i^{\text{pt}}[\Lambda_i + \epsilon; r]. \quad (4.1)$$

Here, $V_i^{\text{pt}}[\mu; r]$ is the exchange potential for a graph with point (bare) vertex functions, and with the mass parameter m_i replaced by μ . m_i and Λ_i are the Bonn mass and cutoff parameters, and ϵ is an arbitrary small expansion parameter. (We use $\epsilon \leq 10$ MeV.)

Desplanques, Donoghue, and Holstein¹⁰ (DDH) applied the quark and Weinberg-Salam models to estimate the parity-violating coupling constants. Their results for the nonrelativistic one-meson-exchange point vertex potentials for two protons are

power \hat{A} and the angular analyzing power $A(\theta)$ are indicated as solid curves in Figs. 1 and 2. The results were obtained using, in Eq. (2.4), model-derived values for $\hat{\gamma}_W$, determined as described in the Appendix, and empirical values for $\hat{\gamma}_S$, obtained from Arndt's analysis of conventional scattering data.²¹ The various curves in Figs. 1 and 2 were obtained using alternative distorting potentials^{20,22–25} V_S . In one case, $V_S = 0$, and the distorted waves become pure Coulomb functions. In all of the cases, V_W uses Bonn parameter values and form factors,

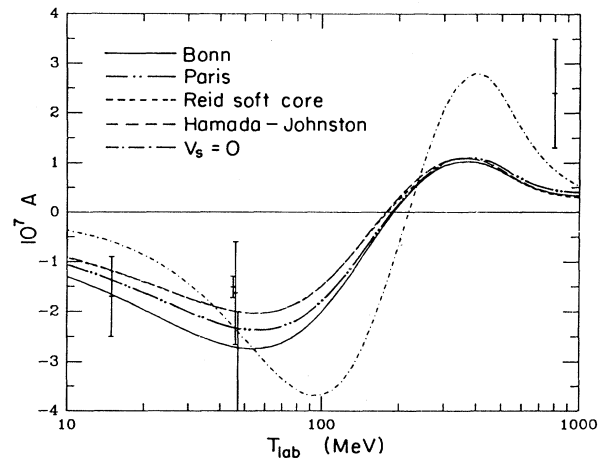


FIG. 1. The reduced analyzing power \hat{A} , Eq. (3.17), using various potential models V_S for calculating the distorted waves $u^{(s)}$ in Eq. (A7). The experimental data are from Refs. 1–5.

and V_W remains fixed.

Long-range Coulomb effects are included in the angular analyzing power results of Fig. 2. The Coulomb amplitude dominates at small scattering angles θ and causes $A(\theta)$, Eq. (3.3), to change sign, and then vanish, as θ decreases to zero. The reduced total analyzing power \hat{A} , on the other hand, is influenced by Coulomb repulsion only within short, nuclear ranges.

Figures 3(a) and (b) are plots of the integrand of the DWBA integral, Eq. (A7), at the laboratory kinetic energies of 45 and 230 MeV for the case $j=0$. The various curves are obtained using standing distorted waves $u^{(s)}(r)$ (see the Appendix) generated by different strong potentials V_S , or with $V_S=0$, as indicated in the legend of Fig. 1. The curves for the Hamada-Johnston potential begin at the hard-core radius. The abscissa coordinate r is the separation between protons. Although the rho and omega ranges are only 0.25 fm, the contributing separation distances, for all the nontrivial distorting potentials

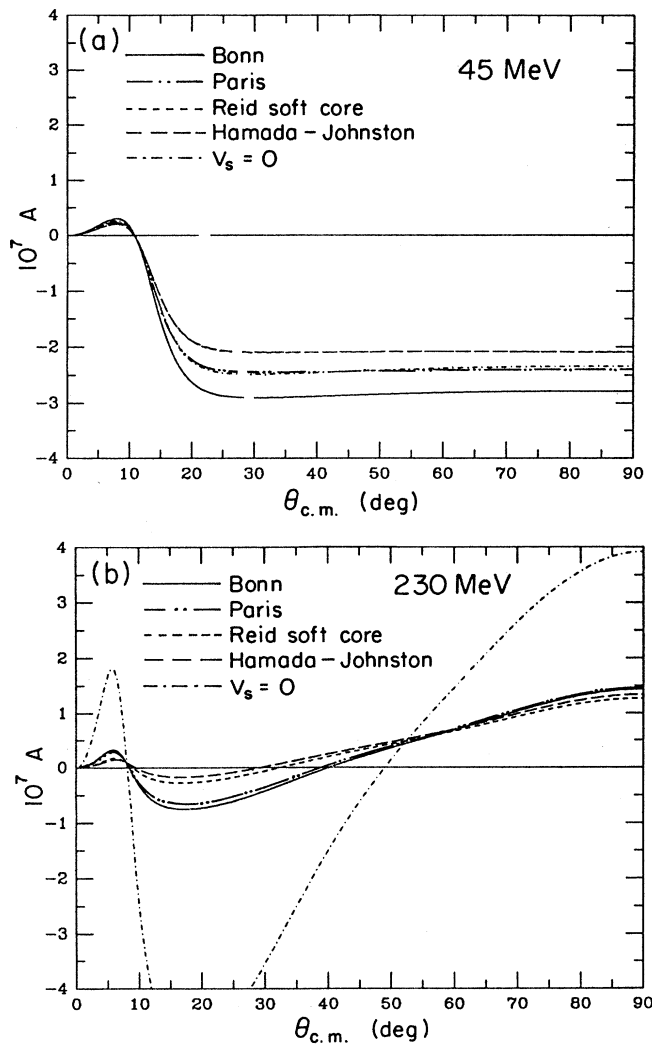


FIG. 2. (a) The angular analyzing power, Eq. (3.3), at the proton lab kinetic energy 45 MeV; (b) same as (a), but at 230 MeV.

shown, are much larger. Short-range repulsive forces, or a hard core, exclude the distorted waves from the smaller distances.

As an alternative to Arndt's t -matrix values, \hat{t}_S can be derived from the same solutions of the strong potential as used in calculating \hat{t}_W . These derived values of \hat{t}_S , however, generally disagree with Arndt's values and lead to inconsistent predictions. In particular, the helicity-independent cross section and the zero crossing energy of the helicity-dependent cross section are determined less accurately from the model-derived values of \hat{t}_S than from Arndt's empirical values.

Figure 4 illustrates the discrepancies between analyzing power predictions using the alternative values for \hat{t}_S . Part (a) shows various predictions using the Bonn potential, and part (b) using the Paris potential. The solid curves in Fig. 4 are the results of Fig. 1 for the Bonn and Paris potentials, where Arndt's matrix elements were used. The dash-dot-dotted curves use model-derived values of \hat{t}_S in Eq. (2.4) to calculate \hat{t}_W , which determines

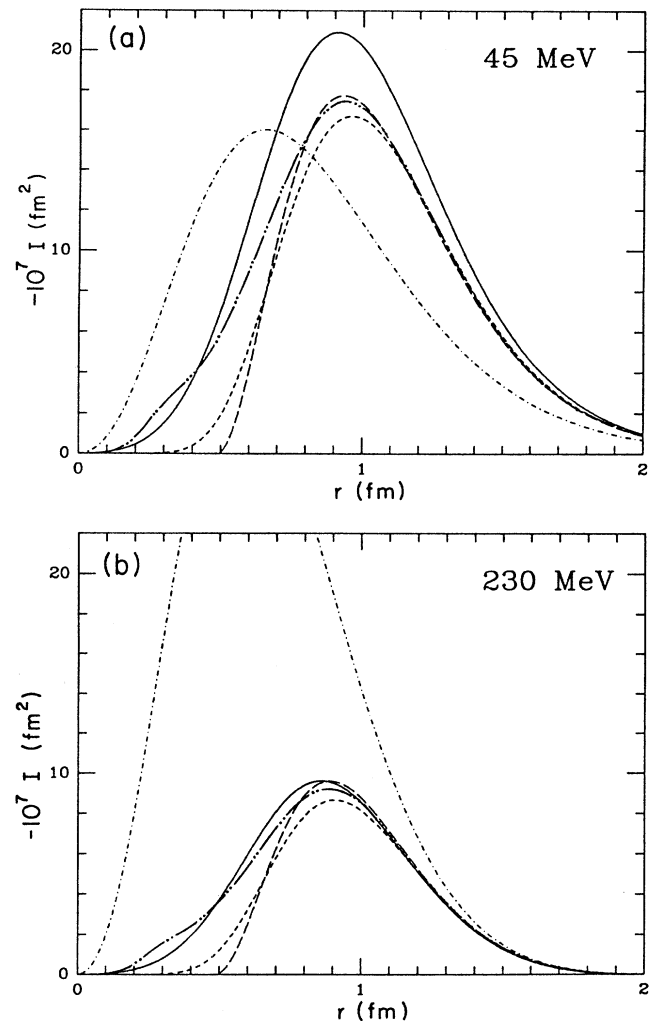


FIG. 3. (a) The $j=0$ transition element of the integrand of the DWBA integral, Eq. (A7). The proton lab kinetic energy is 45 MeV; (b) same as (a), but at 230 MeV.

the helicity-dependent cross section, but use Arndt's values to calculate the helicity-independent cross section. The dashed curves use model-derived values in both cross sections.

We observe larger discrepancies between the curves in Fig. 4(a) than in Fig. 4(b). The Bonn potential produces larger inconsistencies because the Bonn model was adjusted to fit np scattering data, not pp data, so the Bonn model produces less accurate pp phase shifts than the Paris potential. Notice, also, in Fig. 1 that the Bonn and Paris distorted waves produce a difference in \hat{A} comparable to the differences in Fig. 4(a) induced by the errors in the Bonn values for \hat{t}_S . Above inelastic threshold, inelastic contributions to helicity-independent cross sections reduce the analyzing power by as much as a factor of 2. Inelastic contributions to helicity-dependent cross sections through the strong factors in Eq. (2.4) are insignificant.

Figure 5 shows the effect of "switching off" the absorptive components of Arndt's amplitudes. The nominal prediction of Fig. 1, using Arndt's absorptive matrix elements, is shown again as a solid curve. The effect of set-

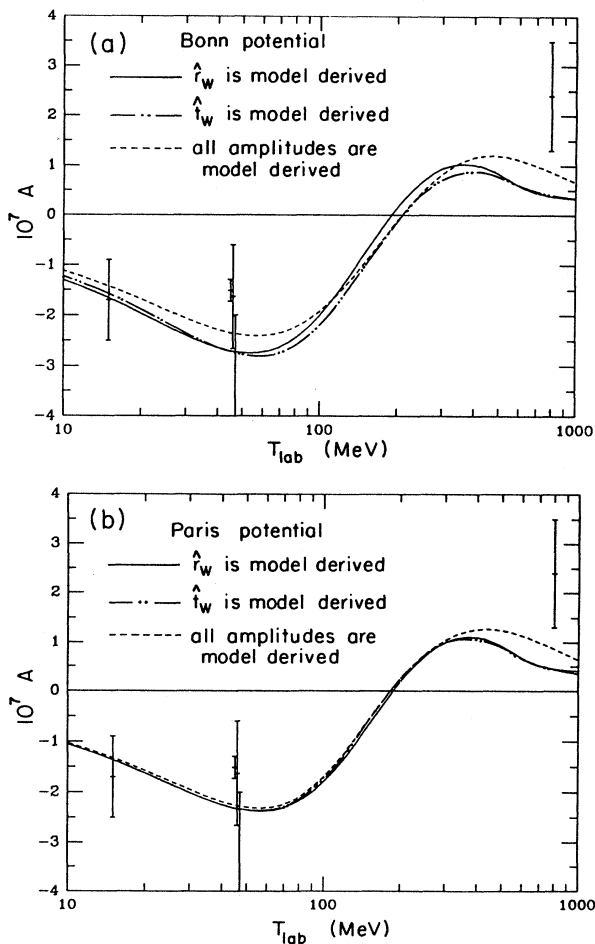


FIG. 4. (a) The reduced analyzing power, using Bonn distorted waves and alternative theoretical and empirical values for the on-shell t matrix \hat{t}_S ; (b) same as (a), but using Paris distorted waves.

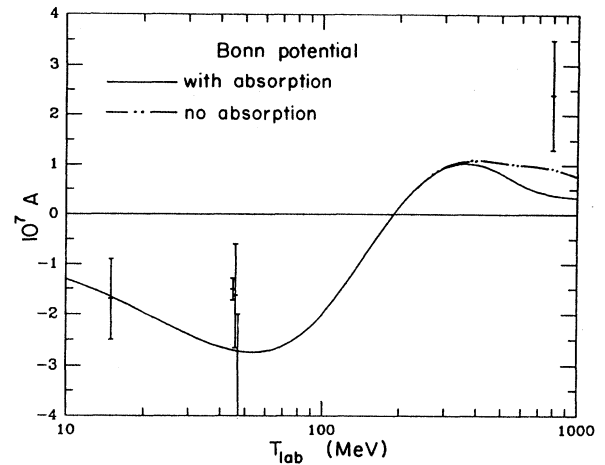


FIG. 5. The effect of "switching off" absorptive components of Arndt's t -matrix elements.

ting the imaginary part of \hat{p}_S , related to \hat{t}_S in Eq. (2.1'), to zero is shown as a dash-dot-dotted curve.

Figures 6–10 show the contributions of separate partial-wave matrix elements of \hat{p}_W , of separate terms of the parity-violating potential V_W , and of the form-factor modifications to V_W . The analyzing power, \hat{A} or $A(\theta)$, depends linearly on the matrix elements of \hat{p}_W , and linearly on the separate terms of V_W .

Figures 6 and 7 show the separate contributions of the three independent elements of \hat{p}_W with $j \leq 2$. The solid curve, the nominal prediction for \hat{A} , is the sum of all contributions with $j \leq 6$. In all the cases, all partial-wave matrix elements of \hat{t}_S in Arndt's analysis are included in the helicity-independent cross section. At low energies through $T_{lab} \approx 50$ MeV, only the 1S_0 - 3P_0 parity-violating transition contributes; above 50 MeV, only one additional transition becomes important.

The weak potential, including the form-factor contributions defined in Sec. IV, can be separated into four terms, two associated with the rho meson, and two with the omega meson. For each meson, one term includes all

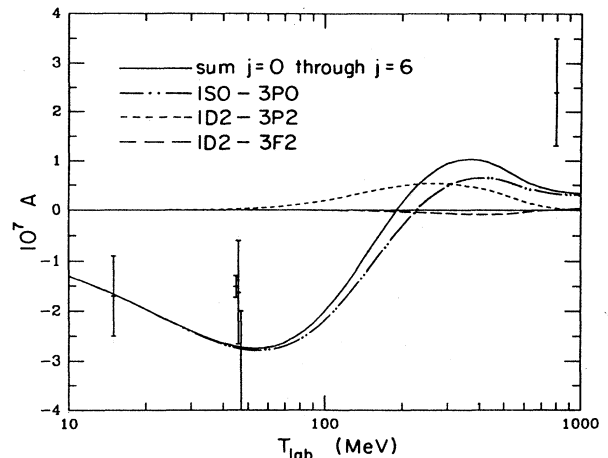


FIG. 6. Contributions of $j=0$ and $j=2$ elements of \hat{p}_W to the reduced analyzing power.

operators \mathcal{O}_a , and one all operators \mathcal{O}_b , where \mathcal{O}_a and \mathcal{O}_b are defined in Eq. (A9), with m a meson or cutoff mass. Figure 8 shows the contributions of the rho and omega terms, and of the separate a - and b -type rho terms. For the DDH "best values" of h_ρ^{pp} and h_ω^{pp} , the a -type rho operator dominates.

Figure 9 compares the "bare" rho Yukawa with the "effective" rho Yukawa obtained by adding higher mass terms, as prescribed by the Bonn form-factor modification, Eq. (4.1). Figure 10 demonstrates the effect of the form-factor modifications of $V_{W\rho}$ and $V_{W\omega}$ on \hat{A} . For this comparison, V_S and its form factors are not changed. The solid curve, the Bonn prediction of Fig. 1, includes the modification of V_W using the nominal values $\Lambda_\rho = 1300$ MeV and $\Lambda_\omega = 1500$ MeV. For the dash-dot-dotted curve, the values Λ_ρ and Λ_ω are increased in V_W by 100 MeV. For the dashed curve, V_W is unmodified.

The Bonn form-factor modifications to V_W reduce the

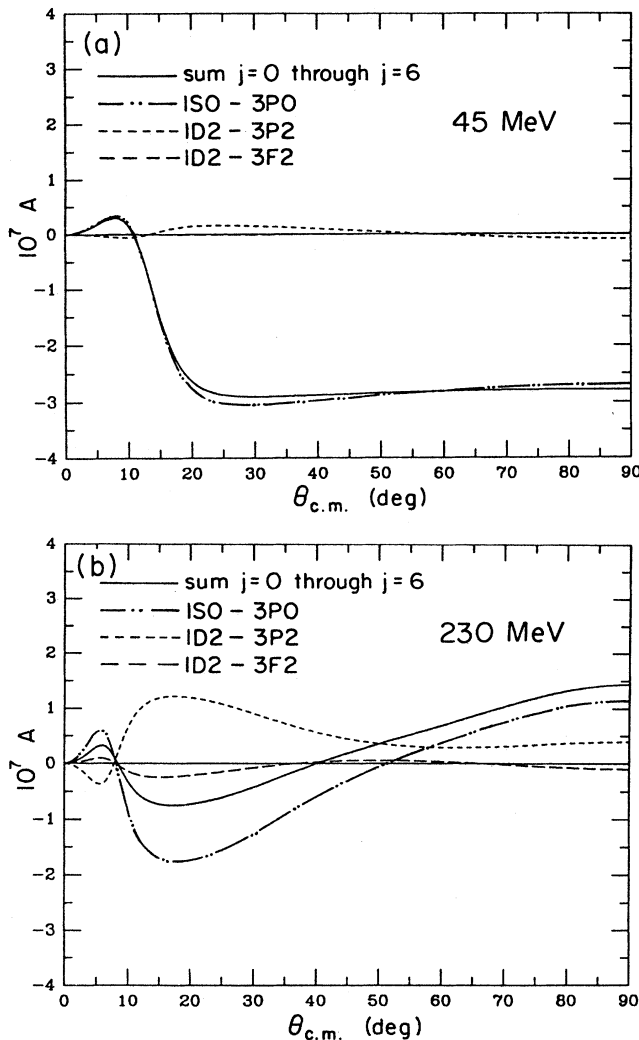


FIG. 7. (a) Contributions of $j=0$ and $j=2$ elements of \hat{r}_W to the angular analyzing power at the proton lab kinetic energy 45 MeV; (b) same as (a), but at 230 MeV.

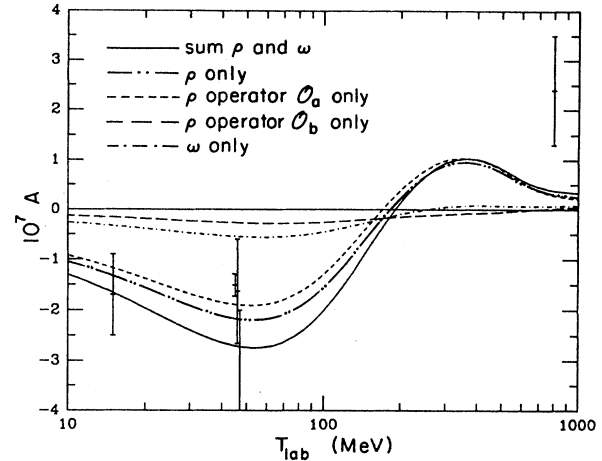


FIG. 8. The rho and omega parity-violating exchange contributions, and the separate contributions of operators \mathcal{O}_a and \mathcal{O}_b in rho exchange.

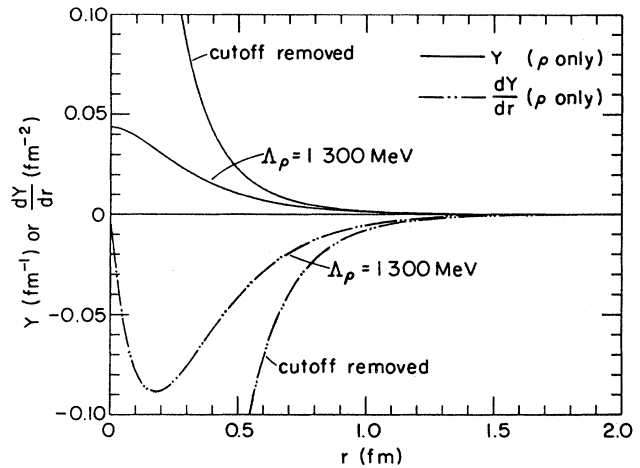


FIG. 9. The rho Yukawa $e^{-m_\rho r}/4\pi r$ (solid lines) and derivative (dash-dot-dotted lines), with and without Bonn form-factor modifications. The unmodified functions are those diverging at $r \rightarrow 0$.

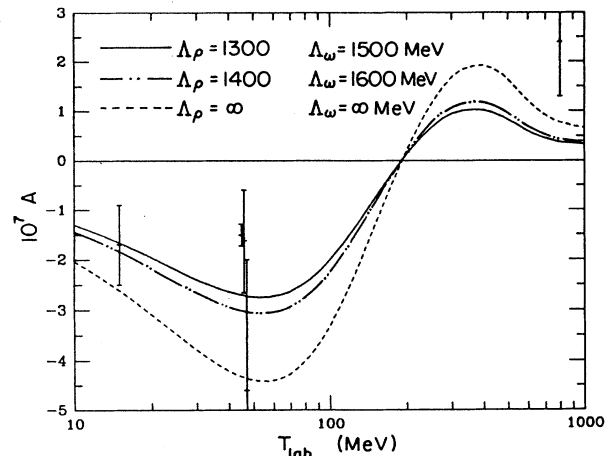


FIG. 10. The effect of varying the cutoff parameters Λ_ρ and Λ_ω in the parity-violating potential.

analyzing power by, roughly, an energy- and angle-independent factor of 1.7. As was shown in Fig. 3, only separations in the range 0.6–1.2 fm contribute to the parity-violating observables. At these relevant distances, the Yukawa is reduced, roughly, by the factor 1.7. The distorted waves do not sense the extreme change in shape of the Yukawa at shorter ranges.

Figures 11 and 12 show the effects of Coulomb contributions to various theoretical and observable total cross sections. Figure 11 compares the theoretical total analyzing powers \hat{A} , $A|_N$, and $A|_{\eta=0}$, where \hat{A} is defined by Eq. (3.17), where

$$A|_N = \frac{\sigma_{+|N} - \sigma_{-|N}}{\sigma_{+|N} + \sigma_{-|N}}, \quad (5.1)$$

and where $A|_{\eta=0}$ is obtained by setting the Coulomb parameter in all factors to zero. Figure 11 shows that Coulomb-nuclear interference and short-range Coulomb distortion effects on the total cross sections are small above 10 MeV.

Pure Coulomb contributions can, however, be significant in observed total cross sections if the detector angle θ_d is small. The effect on the angular analyzing power $A(\theta)$ at small scattering angles is shown in Fig. 2. Figure 12 compares the predicted observable

$$A|_{>\theta_d} = \frac{\sigma_{+|>\theta_d} - \sigma_{-|>\theta_d}}{\sigma_{+|>\theta_d} + \sigma_{-|>\theta_d}} \quad (5.2)$$

for transmission experiments for various values of θ_d . Below the inelastic threshold, the cross sections are calculated by integrating differential cross sections over angles larger than θ_d . Above the inelastic threshold, the Holdeman-Thaler modified optical theorem, Eqs. (3.9) and (3.12), is needed to include inelastic contributions to the cross sections. The discontinuity of the curves at 300 MeV is a consequence of neglecting $|M_N|^2$ at small angles and of neglecting nonisotropic partial waves in Eq. (3.12).

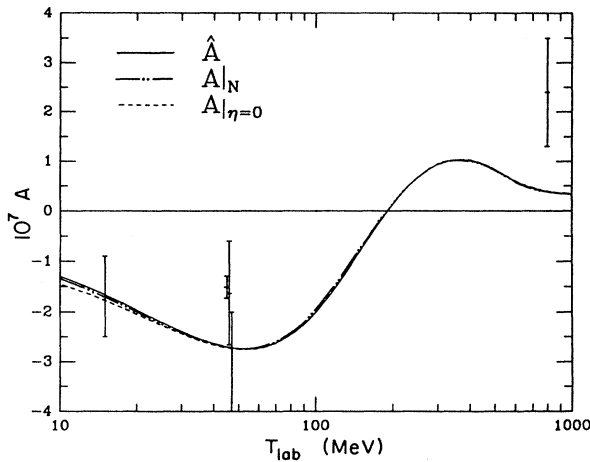


FIG. 11. Comparison of the reduced and nuclear analyzing powers, and the analyzing power with Coulomb effects completely neglected ($\eta=0$).

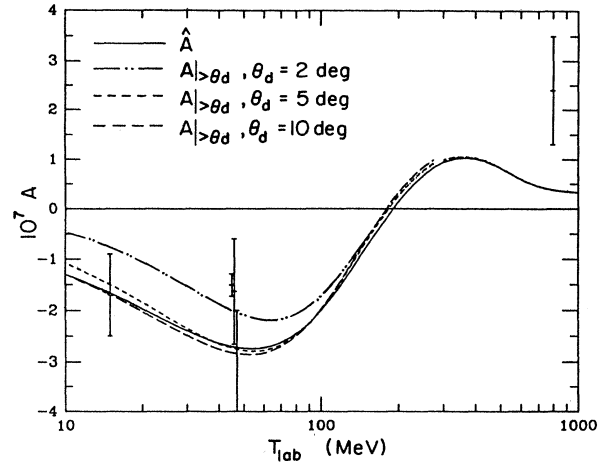


FIG. 12. The reduced analyzing power \hat{A} compared with the predicted observable $A|_{>\theta_d}$ defined by Eqs. (3.9) and (3.12). The specified angles are θ_d in the lab frame.

With these approximations, the Holdeman-Thaler result differs only slightly, above inelastic threshold, with the reduced analyzing power \hat{A} .

VI. SUMMARY

We derive and employ a new expression for the weak t matrix, Eq. (2.4), which reduces the model dependence of the parity-violating observables to the weak r matrix, \hat{r}_W . Below pion production threshold, \hat{r}_W is real and symmetric and becomes a real DWBA matrix element, Eq. (A7). Inelastic effects can be incorporated in the phenomenological strong factors in Eq. (2.4) for \hat{r}_W . The effect of inelastic contributions in the factors $(1 + \hat{u}_S)$ of \hat{r}_W , however, is small. Inelastic contributions to the helicity-independent cross section, on the contrary, reduce the analyzing power at 800 MeV by roughly a factor of 2. A complete calculation of inelastic effects would require calculating inelastic contributions to the model-derived factor \hat{r}_W , as well.

Figure 13 compares our result using the Bonn potential for \hat{A} (the solid curve, taken from Fig. 1) with earlier work by Brown, Henley, and Krejs,⁸ by Henley and Krejs,¹³ and by Oka.⁹ Brown, Henley, and Krejs use non-relativistic distorted waves derived from the Hamada-Johnston potential. We plot their results (asterisks), for single ρ and ω exchange, multiplied by -1 . The calculations by Henley and Krejs (bars) and Oka (dashed curve) are relativistic, but both neglect distortions. From Ref. 13, we plot the result, multiplied by -1 , for ρ and ω exchange with $f_\omega g_\omega = \sqrt{2} f_\rho g_\rho$. From Ref. 9, we take the larger of two split curves for the case using DDH and vector-meson-universality coupling parameters.

The dominant differences between our result and that of Brown, Henley, and Krejs are the larger values employed in our work for the strong-coupling constants, and the inclusion of form factors. The new coupling constants, especially g_ρ and μ_V , increase the magnitude of \hat{A} .

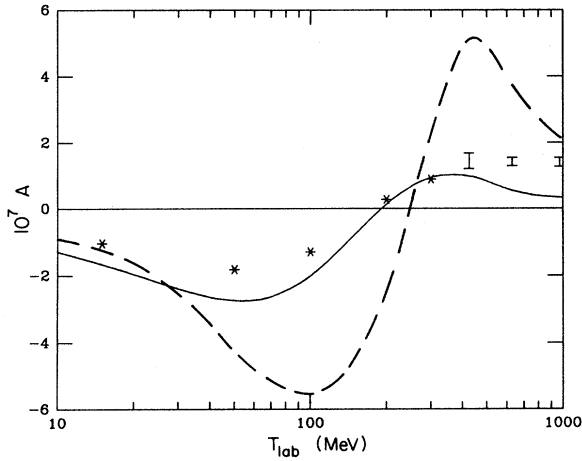


FIG. 13. Comparison of our analyzing power prediction with predictions of Brown, Henley, and Krejs (Ref. 8), of Henley and Krejs (Ref. 13), and of Oka (Ref. 9). The figure is explained in the text.

The use of form factors, new to this work, tends to compensate by reducing the magnitude of \hat{A} .

Oka's result for \hat{A} is qualitatively similar, but not equivalent, to our own for $V_S=0$ [Fig. 1(a), the dash-dotted curve]. Oka's parametrization, similar to that of Henley and Krejs, for the S matrix differs from our own formulation, Eqs. (2.2') and (2.4). With inaccurate distortions of the weak amplitudes (or with no distortions), the formulas disagree by factors depending on the strong phase shifts, and so produce different predictions for \hat{A} and its energy dependence. The analyzing-power predictions also differ due to differences in the strong-coupling parameters, the modification (in our work) of V_W by form factors, and the relativistic treatment of V_W in Oka's work and that of Henley and Krejs.

$$\psi_{s'm'_s;sm_s}(\mathbf{r};\mathbf{k}) = 4\pi \sum_{j'l'} i^{l'} \frac{u_{l's';ls}^j(r;k)}{r} \sum_{m_j} \mathcal{Y}_{j(l's')m_j}^{m'_s}(\hat{\mathbf{r}}) \mathcal{Y}_{j(ls)m_j}^{m_s*}(\hat{\mathbf{k}}), \quad (\text{A1})$$

where

$$\mathcal{Y}_{j(ls)m_j}^{m_s} \equiv \sum_{m_l} C_{jls}^{m_j m_l m_s} Y_l^{m_l}$$

are the spinor elements of the vector spherical harmonics. The partial-wave components $v_{l's';ls}^j$ of a potential V are determined by (A1). Let $\psi' = V\psi$ be the function obtained by operating with V on the function ψ of (A1), and let $u_{l's';ls}^j$ be the radial wave functions related to $\psi_{l's';ls}^j$ by the same formula (A1). Then,

$$u_{l's';ls}^j = \sum_{l''s''} v_{l's';l''s''}^j u_{l''s'';ls}^j. \quad (\text{A2})$$

Each element $v_{l's';ls}^j$ is an operator which acts on func-

The analyzing power results depend linearly on two parity-violating parameters h_ρ^{pp} and h_ω^{pp} . Three or more precise measurements of the analyzing power are required to fix h_ρ^{pp} and h_ω^{pp} (or their product with strong-coupling parameters) and to test the meson-exchange model.

Generally, Coulomb corrections to the analyzing power are found to be small. However these can be as large as $\sim 10^{-8}$ when $T_{\text{lab}} \lesssim 300$ MeV, or for transmission experiments sensitive to laboratory scattering angles of 5 deg or less. These corrections are comparable to the sensitivity claimed for some experiments.^{2,7} Three different theoretical cross sections, \hat{A} , A_N , and $A|_{\eta=0}$, obtained by three different methods for removing the Coulomb cross-section singularities, differ significantly only below 40 MeV.

This work was supported in part by the U.S. Department of Energy.

APPENDIX

We calculate the matrix elements $\hat{r}_{Wl's';ls}^j$ by the distorted-wave method using parity-conserving Coulomb and strong distorting potentials V_C and V_S and a parity-violating perturbing potential V_W . The integrations used in obtaining the distorted waves and the real DWBA integrals are described in this Appendix.

The integrations and calculation of $\hat{r}_{Wl's';ls}^j$ are performed in a partial wave representation using radial wave functions $u_{l's';ls}^j(r;k)$. Let $\psi_{s'm'_s;sm_s}(\mathbf{r};\mathbf{k})$ be a solution of the scattering wave equation with spatial coordinates \mathbf{r} , spin components s' and m'_s , and boundary conditions (either incoming, outgoing, or standing wave) with quantum numbers \mathbf{k} , s , and m_s . The radial wave functions $u_{l's';ls}^j(r;k)$ are defined by the partial-wave expansion

tions of the radial coordinate r . For simplicity, we assume matrix notation when the indices are suppressed. For example, (A2) is written simply as $u' = vu$.

The representation defined by (A1) and (A2) is different from a convention, commonly adopted in the literature,^{20,22,23,25,26} that uses a phase factor $i^{l'}$ in Eq. (A1) rather than $i^{l''}$. In our representation, the partial-wave coordinate representation v_W for V_W is real and symmetric. In the alternative representation, v_W is pure imaginary and antisymmetric. To preserve the symmetry and reality of matrix expressions in our formalism, we adopt (A1).

The first step in calculating \hat{r}_W is to solve Schrödinger's equation

$$\left[\frac{-1}{m_N} \left[\frac{d^2}{dr^2} - \frac{L^2}{r^2} \right] + v_C + v_S \right] u = \frac{k^2}{m_N} u, \quad (\text{A3})$$

with the interior boundary condition

$$\lim_{r \rightarrow 0} u(r; k) = 0, \quad (\text{A4a})$$

for soft-core potentials V_S , or

$$u(r_{\text{core}}; k) = 0, \quad (\text{A4b})$$

for hard-core potentials. Three solution sets, identified by superscripts (+), (s), and (-) to denote outgoing, standing-wave, and incoming boundary conditions, are determined by Eqs. (A3) and (A4) and an additional boundary condition outside the range d of V_S :

$$u_{l's';ls}^{(+)}(r; k) \sim \frac{1}{r > d} \frac{1}{2ik} \left[-\delta_{l'l} \delta_{s's} H_l^{(-)}(kr) + \hat{s}_{l's';ls}^j H_l^{(+)}(kr) \right], \quad (\text{A5a})$$

$$u_{l's';ls}^{(s)}(r; k) \sim \frac{1}{r > d} \frac{1}{k} \left[\delta_{l'l} \delta_{s's} F_l(kr) + \hat{r}_{l's';ls}^j G_l(kr) \right], \quad (\text{A5b})$$

$$u_{l's';ls}^{(-)}(r; k) \sim -\frac{1}{r > d} \frac{1}{2ik} \left[\hat{s}_{l's';ls}^{-1j} H_l^{(-)}(kr) - \delta_{l'l} \delta_{s's} H_l^{(+)}(kr) \right]. \quad (\text{A5c})$$

Here, F_l and G_l are the regular and irregular Coulomb functions with asymptotic forms

$$F_l(kr) \underset{kr \rightarrow \infty}{\sim} \sin \left[kr - \frac{l\pi}{2} - \eta \ln(2kr) + \sigma_l \right], \quad (\text{A6a})$$

$$G_l(kr) \underset{kr \rightarrow \infty}{\sim} \cos \left[kr - \frac{l\pi}{2} - \eta \ln(2kr) + \sigma_l \right], \quad (\text{A6b})$$

and

$$H_l^{\pm} \equiv G_l \pm i F_l. \quad (\text{A6c})$$

The coefficients \hat{s}_S , \hat{r}_S , and \hat{s}_S^{-1} in Eq. (A5) are not independently specified quantities. They are determined uniquely with solutions $u^{(+)}$, $u^{(s)}$, and $u^{(-)}$ by the condition Eq. (A4) and by the Kronecker δ -function coefficients in Eqs. (A5a), (A5b), and (A5c). Notice that $u^{(+)} = u^{(s)}(1 + i\hat{t}_S) = u^{(-)}\hat{s}_S$.

The real DWBA formula for \hat{r}_W is

$$\hat{r}_W = -m_N k \int dr u^{(s)} v_W u^{(s)}, \quad (\text{A7})$$

where, again, we employ the compact notation described following Eq. (A2). The normalization of Eq. (A7) agrees with Eqs. (2.1') and (2.2'). The parity-violating t -matrix elements are then determined from \hat{r}_W and \hat{t}_S by Eq. (2.4). Alternatively, \hat{t}_W can be calculated directly from

$$\hat{t}_W = -m_N k \int dr u^{(-)\dagger} v_W u^{(+)}. \quad (\text{A8})$$

Comparing Eqs. (A5) and (A6), with the relation $\hat{s}_S = 1 + 2i\hat{t}_S$, it is simple to show that Eqs. (A7) and (A8) are consistent with Eq. (2.4).

Notice that the normalization for $u^{(s)}$ in Eq. (A7) and defined by Eq. (A5b) differs from another normalization commonly assumed for standing-wave radial functions. For uncoupled channels, when $\hat{r}_{l's';ls}^j = \delta_{l'l} \delta_{s's} \tan \delta_l$, the solutions $u^{(s)}$ have, by Eqs. (A5b) and (A6b), the asymptotic form

$$u_{l's';ls}^{(s)} \underset{kr \rightarrow \infty}{\sim} \frac{A}{k} \sin \left[kr - \frac{l\pi}{2} - \eta \ln(2kr) + \delta_l + \sigma_l \right],$$

with $A = (\cos \delta_l)^{-1}$, not $A = 1$. The normalization defined by Eq. (A5b), however, is related to $u^{(+)}$ in Eq. (A5a) by the factor $1 + i\hat{t}_S$. In the outside region $r \gg d$, the standing wave Green's function contributes only irregular Coulomb function components to $u^{(s)}$. In the three asymptotic forms (A5) for $u^{(+)}$, $u^{(s)}$, and $u^{(-)}$, the coefficients for $H_l^{(-)}$, F_l , and $H_l^{(+)}$, respectively, are specified and do not depend on v_S ; all degrees of freedom in the asymptotic forms that depend on v_S are contained in \hat{s}_S , \hat{r}_S , or \hat{s}_S^{-1} . For other normalization choices, especially for coupled channels, the relationships of the asymptotic coefficients to v_S are more complicated.

The remaining quantity v_W in Eq. (A7) is the partial-wave representation of V_W , with V_W defined by Eqs. (4.2) and (4.1). V_W is a linear combination of the parity-violating operators

$$\begin{aligned} \mathcal{O}_a(m) &= i(\sigma_1 \times \sigma_2) \cdot \left[\mathbf{p}, \frac{e^{-mr}}{4\pi r} \right], \\ \mathcal{O}_b(m) &= (\sigma_1 - \sigma_2) \cdot \left[\mathbf{p}, \frac{e^{-mr}}{4\pi r} \right], \end{aligned} \quad (\text{A9})$$

where m is a mass. Then v_W is the same linear combination of the partial-wave representations of \mathcal{O}_a and \mathcal{O}_b ,

$$\begin{aligned} \mathcal{O}_{aj0;j-11}^j &= \mathcal{O}_{aj-11;j0}^j = 2 \left[\frac{j}{2j+1} \right]^{1/2} \frac{dY}{dr}, \\ \mathcal{O}_{aj0;j+11}^j &= \mathcal{O}_{aj+11;j0}^j = 2 \left[\frac{j+1}{2j+1} \right]^{1/2} \frac{dY}{dr}, \\ \mathcal{O}_{bj0;j-11}^j &= 2 \left[\frac{j}{2j+1} \right]^{1/2} \left[-2Y \frac{d}{dr} - \frac{dY}{dr} + \frac{2j}{r} Y \right], \\ \mathcal{O}_{bj-11;j0}^j &= 2 \left[\frac{j}{2j+1} \right]^{1/2} \left[+2Y \frac{d}{dr} + \frac{dY}{dr} + \frac{2j}{r} Y \right], \\ \mathcal{O}_{bj0;j+11}^j &= 2 \left[\frac{j+1}{2j+1} \right]^{1/2} \left[-2Y \frac{d}{dr} - \frac{dY}{dr} - \frac{2j+2}{r} Y \right], \\ \mathcal{O}_{bj+11;j0}^j &= 2 \left[\frac{j+1}{2j+1} \right]^{1/2} \left[+2Y \frac{d}{dr} + \frac{dY}{dr} - \frac{2j+2}{r} Y \right], \end{aligned} \quad (\text{A10})$$

where $Y = e^{-mr}/4\pi r$. Form factors modify Eqs. (A9) or (A10) according to Eq. (4.1). All elements of \mathcal{O}_a or \mathcal{O}_b not given in Eq. (A10) are zero.

- ¹D. E. Nagle *et al.*, in *High Energy Physics with Polarized Beams and Polarized Targets (Argonne, 1978)*, Proceedings of the Third International Symposium on High Energy Physics with Polarized Beams and Polarized Targets, AIP Conf. Proc. No. 51, edited by G. H. Thomas (AIP, New York, 1979), p. 224.
- ²S. Kistryn *et al.*, *Phys. Rev. Lett.* **58**, 1616 (1987).
- ³P. von Rossen *et al.*, in Proceedings of the Sixth International Symposium on Polarization Phenomena in Nuclear Physics, Osaka, 1985 [J. Phys. Soc. Jpn. Suppl., **55**, 1016 (1986)].
- ⁴D. M. Tanner *et al.*, *Proceedings of the International Conference on Nuclear Physics, 1983* (Tipografia Compositori, Florence, 1983), Vol. 1, p. 697.
- ⁵V. Yuan *et al.*, *Phys. Rev. Lett.* **57**, 1680 (1986).
- ⁶M. Simonius, in *Intersections Between Particle and Nuclear Physics—1986, Lake Louise, Canada*, Proceedings of the Second Conference on the Intersections of Particle and Nuclear Physics, AIP Conf. Proc. No. 150, edited by Donald F. Geesaman (AIP, New York, 1986).
- ⁷J. Birchall, in Proceedings of the Symposium/Workshop on Parity Violation in Hadronic Systems, TRIUMF, Vancouver, 1987, p. 143; S. A. Page, *ibid.*, p. 135.
- ⁸V. R. Brown, E. M. Henley, and F. R. Krejs, *Phys. Rev. C* **9**, 935 (1974).
- ⁹T. Oka, *Prog. Theor. Phys.* **66**, 977 (1981).
- ¹⁰B. Desplanques, J. F. Donoghue, and B. R. Holstein, *Ann. Phys. (N.Y.)* **124**, 449 (1980).
- ¹¹E. G. Adelberger and W. C. Haxton, *Annu. Rev. Nucl. Part. Sci.* **35**, 501 (1985).
- ¹²E. M. Henley, *Nucl. Phys.* **A483**, 596 (1988).
- ¹³E. M. Henley, and F. R. Krejs, *Phys. Rev. D* **11**, 605 (1975).
- ¹⁴K. M. Watson, *Phys. Rev.* **95**, 228 (1954).
- ¹⁵M. L. Goldberger and K. M. Watson, *Collision Theory* (Krieger, Huntington, N.Y., 1975).
- ¹⁶A. Messiah, *Quantum Mechanics* (North-Holland, Amsterdam, 1958).
- ¹⁷J. T. Holdeman and R. M. Thaler, *Phys. Rev. Lett.* **14**, 81 (1965); *Phys. Rev.* **139**, B1186 (1965).
- ¹⁸M. D. Cooper and M. B. Johnson, *Nucl. Phys.* **A260**, 352 (1976).
- ¹⁹A. S. Goldhaber, *Phys. Rev. D* **25**, 715 (1982).
- ²⁰R. Machleidt, K. Holinde, and Ch. Elster, *Phys. Rep.* **149**, No. 1, (1987). The coordinate-representation one-boson-exchange Bonn potential is identified as OBEPR in this reference.
- ²¹R. A. Arndt, J. S. Hyslop III, and L. D. Roper, *Phys. Rev. D* **35**, 128 (1987).
- ²²M. Lacombe *et al.*, *Phys. Rev. C* **21**, 861 (1980).
- ²³R. V. Reid, *Ann. Phys. (N.Y.)* **50**, 411 (1968).
- ²⁴B. D. Day, *Phys. Rev. C* **24**, 1203 (1981). A prescription for extending the Reid potential, Ref. 18, to partial waves with $j > 2$ is defined in the Appendix.
- ²⁵T. Hamada and I. D. Johnston, *Nucl. Phys.* **34**, 382 (1962).
- ²⁶J. M. Blatt and L. C. Biedenharn, *Phys. Rev.* **86**, 399 (1952).